Acta Neuropathol
DOI 10.1007/s00401-011-0877-0

ORIGINAL PAPER

Homeostatic responses by surviving cortical pyramidal cells in neurodegenerative tauopathy

Johanna L. Crimins · Anne B. Rocher · Alan Peters · Penny Shultz · Jada Lewis · Jennifer I. Luebke

Received: 12 August 2011 / Revised: 16 September 2011 / Accepted: 16 September 2011

Abstract Cortical neuron death is prevalent by 9 months in rTg(tau_{P301L})4510 tau mutant mice (TG) and surviving pyramidal cells exhibit dendritic regression and spine loss. We used whole-cell patch-clamp recordings to investigate the impact of these marked structural changes on spontaneous excitatory and inhibitory postsynaptic currents (sEPSCs and sIPSCs) of layer 3 pyramidal cells in frontal cortical slices from behaviorally characterized TG and non-transgenic (NT) mice at this age. Frontal lobe function of TG mice was intact following a short delay interval but impaired following a long delay interval in an object recognition test, and cortical atrophy and cell loss were pronounced. Surviving TG cells had significantly reduced dendritic diameters, total spine density, and mushroom spines, yet sEPSCs were increased and sIPSCs were unchanged in frequency. Thus, despite significant regressive structural changes, synaptic responses were not reduced in TG cells, indicating that homeostatic compensatory mechanisms occur during progressive tauopathy. Consistent with this idea, surviving TG cells were more intrinsically excitable than NT cells, and exhibited sprouting of filopodia and axonal boutons. Moreover, the neuropil in TG mice showed an increased density of asymmetric synapses, although their mean size was reduced. Taken together, these data indicate that during progressive tauopathy, cortical pyramidal cells compensate for loss of afferent input by increased excitability and establishment of new synapses. These compensatory homeostatic mechanisms may play an important role in slowing the progression of neuronal network dysfunction during neurodegenerative tauopathies.

Keywords In vitro slice · Whole-cell patch clamp · Dendritic spines · Synaptic physiology · Axonal boutons

Introduction

Synaptic dysfunction during progressive tauopathy contributes significantly to cognitive decline (review [8, 24]), yet a detailed understanding of synaptic changes during early versus advanced stages of pathology is lacking. At early stages of tauopathy (before cortical neuronal death) in 4-month-old rTg4510 mice, mislocalization of hyperphosphorylated tau to spines of hippocampal pyramidal cells causes removal of GluR1 AMPA receptors from spines and decreased AMPA receptor-mediated synaptic currents [9]. Prolonged absence of AMPA receptors leads to regression of spines [14], so this initial loss of receptors may lead to spine loss as tauopathy progresses. Indeed, significant spine loss and dendritic regression occur in cortical pyramidal cells of ~9-month-old rTg4510 mice [28] and in hippocampal pyramidal cells transfected with mutant tau [41].

The functional consequences of neuron death (deafferentation) and localized structural changes on synaptic responses of surviving neurons at advanced stages of tauopathy are poorly understood. While a decrease in long-term potentiation in hippocampal neurons has been consistently

J. L. Crimins and A. B. Rocher contributed equally to this work.

J. L. Crimins · A. B. Rocher · A. Peters · P. Shultz · J. I. Luebke (✉)
M949, Department of Anatomy and Neurobiology, Boston University School of Medicine, 85 East Newton Street, Boston, MA 02118, USA
e-mail: jluebke@bu.edu

J. Lewis
Department of Neuroscience, Center for Translational Research in Neurodegenerative Disease, University of Florida, Gainesville, FL, USA

Published online: 04 October 2011

observed in mouse models of tauopathy [22, 37, 46], effects on baseline glutamatergic transmission are equivocal. Thus decreased [46], increased [22] or unchanged [37] baseline field excitatory postsynaptic potential responses have been reported in the hippocampus of P301S, htau, and pro-aggregant models during advanced-stage tauopathy.

There are pathological changes to both presynaptic and postsynaptic structures in the cortex of 9-month-old rTg4510 mice that would be expected to lead to significant synaptic dysfunction. On the presynaptic side, a loss of ~50% of cortical neurons occurs [36], resulting in significant deafferentation of surviving neurons. As the number of synaptic inputs to surviving neurons decreases, this could plausibly lead to postsynaptic changes, including dendrite and spine regression [28] and an attenuation of synaptic signal, as observed in the hippocampus of P301S tau transgenic mice [46]. On the other hand, it is possible that there is a maintenance or even an increase in synaptic signaling, as indicated by studies in htau and pro-aggregant tau mice [22, 37]. If the latter were the case, there would have to be activation of compensatory mechanisms in surviving neurons and networks. Indeed such homeostatic compensation likely occurs during progressive tauopathies such as Alzheimer's disease, accounting for the slow time course of these diseases [35]. Homeostatic maintenance of signal strength has been demonstrated both when excitatory input is increased and when, as in tauopathy, it is decreased (reviews [43, 44]). In this study, we sought to determine whether compensatory mechanisms enable maintained synaptic function in cortical pyramidal cells at an advanced stage of tauopathy.

Materials and methods

Experimental subjects

Eight rTg(tau_{P301L})4510 (TG) [27, 32] and seven age-matched non-transgenic (NT) mice (8.5–9.5 months of age) on the F1 FVB/129 background were used in this study. Six TG and six NT mice were used for combined behavioral, electrophysiological and morphological analyses, and two TG and one NT mice were used for electron microscopy. Mice were maintained in a pathogen-free barrier facility with a 12 h light/dark cycle and given ad libitum access to food and water. Animal use and care were conducted in strict accordance with standards set forth by the National Institutes of Health *Guide for the Care and Use of Laboratory Animals* and the United States *Public Health Service Policy on Humane Care and Use of Laboratory Animals.* The Mayo Clinic and the Boston University Institutional Animal Care and Use Committees (IACUC) approved all animal procedures.

The object recognition test

The object recognition task (ORT) employed here was first developed by Dere et al. [4] to simultaneously investigate both the memory for particular objects (the "what" component of episodic memory) as well as for their specific locations (the "where", object-in-place type component of episodic memory). Previous findings using the ORT have shown that rodents exhibit a natural predisposition to explore novel objects more than familiar objects [6]. This difference can be used as an index for assessing memory function. Furthermore, mice can remember where an object is located in space and tend to explore an object in a new location more than one that remains in the same place [4]. Recent studies have confirmed that while the "what" component of recognition memory relies upon hippocampal function, the prefrontal cortex is responsible for the "where" component [5]. Thus, to evaluate the functional consequences of alterations to these brain areas in the tau mice, the present ORT combines both an evaluation of the traditional familiarity/recognition memory component following either 5- or 15-min delays with an object-in-place discrimination component to assess the spatial aspect of recognition memory.

Behavioral assessments were conducted in an open-field arena (60 × 60 × 28 cm) constructed of dark grey Plexiglass walls with plastic flooring subdivided into 16 identical quadrants with equal illumination of all parts of the field. The test objects consisted of four identical glass brown bottles referred to as 'Object A' and four identical silver colored aluminum cans referred to as 'Object B.' A video recorder was positioned above the center of the field and captured on film all locomotion and exploratory activity for later scoring.

The test had three phases: two Sample Phases with unique objects associated with each phase and 5 min inter-phase intervals between them, followed by a Recognition/Test Phase (Phase 3). Initially, all subjects were habituated to the testing arena (open field) by placing each mouse individually into the testing arena and allowing it to explore for 15 min per day for 3 consecutive days. Following habituation, the ORT began. During each phase of the ORT, each subject was placed in the center of the testing arena and allowed to explore the four identical objects therein for 5 min. The mouse was then returned to its cage for a 5-min inter-phase delay interval before being placed back in the arena for the next test phase. After each phase, all objects and the open field were wiped clean using a 10% isopropyl alcohol solution to remove any residual olfactory cues. During a testing session, each mouse received the following phase sequence: Sample Phase 1: Exploration of four identical copies of Object A in specific locations within the arena; Sample Phase 2: Exploration of

four identical copies of Object B in different specific locations within the testing arena, and Phase 3: Recognition/Test with two Object A and two Object B: one of each type of object was moved to a novel location within the arena while the other of each type of object was placed in the original position. There was a 5-min delay interval between Phases 1 and 2 (for a final retention interval for Object A of 15 min) and a 5-min delay interval between Phases 2 and 3 of 5 min (for a final retention interval for Object B of 5 min).

Test scoring/statistical analysis

Two independent observers, blind to mouse genotype, reviewed digital footage of each phase of the experiment and measured each subject's object exploration and locomotor activity using a millisecond timer. Object exploration was defined as the amount of time the subject spent with its nose oriented toward an object at a distance of <2 mm. An inter-rater reliability of 80% or better was maintained throughout the scoring of all behavioral data. The change in the amount of object recognition following different delay intervals and treatment conditions (familiarity/temporal component) was calculated using discrimination ratios. These ratios were calculated using Phase 3 (recognition phase) data. The discrimination ratio was calculated by determining the percentage of time each mouse spent exploring each object and then dividing that value by the total amount of time the mouse spent exploring all the objects. These discrimination ratios were then compared within each experimental group using multiple Dunnett two-tailed *t* tests with retention interval (5 or 15 min) and object location (original vs. novel) as factors.

Electrophysiology

Mice were killed by decapitation and their brains rapidly removed and submerged in oxygenated (95% O_2, 5% CO_2) ice-cold Ringer's solution, concentrations (in mM): 25 $NaHCO_3$, 124 NaCl, 1 KCl, 2 KH_2PO_4, 10 glucose, 2.5 $CaCl_2$, 1.3 $MgCl_2$ (pH 7.4; Sigma-Aldrich, St. Louis, MO, USA). Then, a tail clipping was removed for confirmatory PCR genotyping. The frontal cortical hemispheres were dissected free and cut into 300-μm thick acute coronal slices with a vibrating microtome. Slices were equilibrated for 1 h at room temperature (RT) in oxygenated Ringer's solution. Individual slices were positioned in submersion type recording chambers (Harvard Apparatus, Holliston, MA, USA) on Nikon E600 IR-DIC microscopes (IR-DIC; Micro Video Instruments, Avon, MA, USA) stages and continuously perfused with RT oxygenated Ringer's solution (2–2.5 ml/min).

Layer 3 pyramidal cells in the dorsal premotor (frontal) cortex were visualized under IR-DIC optics. For assessment of electrophysiological properties and cell filling, whole-cell patch clamp recordings were conducted as previously described [28, 29]. Electrodes were fabricated on a Flaming and Brown horizontal pipette puller (Model P87, Sutter Instrument, Novato, CA, USA) and filled with potassium methanesulfonate internal solution, concentrations (in mM): 122 KCH_3SO_3, 2 $MgCl_2$, 5 EGTA, 10 NaHEPES, 1% biocytin (pH 7.4; Sigma-Aldrich, St. Louis, MO, USA). In Ringer's solution, pipettes had a resistance of between 3 and 6 MΩ. Data were acquired with "PatchMaster" software (HEKA Elektronik, Lambrecht, Germany) and EPC-9 and EPC-10 amplifiers (HEKA Elektronik, Lambrecht, Germany). Signals were low-pass filtered at 10 kHz.

Spontaneous excitatory postsynaptic currents (sEPSCs) were recorded for 2 min from a holding potential of −80 mV and spontaneous inhibitory postsynaptic currents (sIPSCs) were recorded for 2 min from a holding potential of −40 mV. Glutamate receptor-mediated sEPSCs were blocked by application of the non-NMDA receptor antagonist CNQX (10 μM) but not by the application of the NMDA receptor antagonist APV (20 μM), and were unaltered in the presence of the $GABA_A$-receptor antagonist bicuculline methiodide (BMI, 10 μM). $GABA_A$ receptor-mediated sIPSCs were unaffected by CNQX and APV and fully blocked by 10 μM BMI. Synaptic current data were analyzed using MiniAnalysis (Synaptosoft, Decatur, GA, USA), with the detection threshold set at the maximum of the RMS noise level (5 pA). For each cell, the following characteristics of synaptic events were determined: frequency, amplitude, rise time constant and decay time constant [12, 13]. The rise time constant and the decay time constant were determined by fitting averaged traces to a single exponential function.

Single cell morphometry

During the ~15 min recording period cells were simultaneously filled with 1% biocytin. Following recordings slices were sandwiched between filter paper disks and fixed in 4% paraformaldehyde in 0.1 M phosphate buffered saline (PBS) solution (pH 7.4) for 4 days. Following fixation, slices were rinsed in PBS (3 times, 10 min each) and then placed in 0.1% Triton X-100/PBS for 2 h at RT. Slices were then incubated in Streptavidin-Alexa 546 (1:500; Vector Labs, Burlingame, CA, USA) at 4°C for 2 days. In addition, slices were processed with Thioflavin-S to identify neurofibrillary tangles (NFTs) as previously described [28]. Finally, slices were mounted on slides using Prolong Gold mounting medium (InVitrogen, Eugene, OR, USA) and cover-slipped.

Cells were imaged using a Zeiss LSM-510 confocal laser-scanning microscope, as described in detail previously [28, 29]. Fluorescence emitted by Alexa-546 (Helium/Neon laser excitation) was collected using a 560-nm band pass filter. For assessment of axons and dendritic arbors, filled cells were imaged in their entirety at a resolution of 0.1 × 0.1 × 0.2 µm per voxel with a 210-µm working-distance Plan-Apochromat 40×/1.3 NA oil-immersion objective and 1.5 digital zoom (e.g. Fig. 2). While image quality and resolution was excellent for the 40× scans, higher magnification (100×) scans of individual dendritic segments were required for detailed analyses of dendritic diameter and dendritic spines. For these scans, one basal branch was scanned in its entirety and the middle apical trunk and one branch of the distal-apical tuft were imaged; the proximal third of the apical tree was not analyzed since there were few or no spines present in this location in both TG and NT cells. Dendritic segments were systematically selected for dendritic diameter and spine analyses. The mid-apical segment was defined as the middle third of the main apical trunk, the distal apical dendritic segment was the first second-order dendritic branch of the apical tuft that also reached the pial surface, and the basal dendritic segment was the first complete basilar dendrite arising from the soma that was directly adjacent to the axon. Dendritic segments were imaged at high resolution using a UPlanFl 100×/1.3 NA oil objective lens with a voxel size of 0.022 × 0.022 × 0.1 µm. Each image stack was first deconvolved using Autodeblur (Media Cybernetics, Bethesda, MD, USA) to reduce image blurring in the *z*-plane. For each neuron, stacks were then aligned in 3D and integrated into a single volumetric dataset with Volume Integration and Alignment System (VIAS) software [30].

For automatic 3D reconstruction, the single volumetric dataset produced by VIAS integration for each neuron was imported into the 64-bit version of NeuronStudio [30] (available at: http://www.mssm.edu/cnic). NeuronStudio automatically traced the entire dendritic structure of each cell using a Rayburst-based analysis routine and the resulting reconstruction was exported as a .swc file. After the dendritic arbor .swc was generated, the entire axonal arbor was similarly traced and exported as a separate .swc file for subsequent analyses of axonal bouton densities. Axonal boutons (en passant and terminaux), were manually marked on axon .swc files as they appeared along the axon in NeuronStudio (e.g. Fig. 6). The length and diameter of the neurites were then extracted from .swc files using L-measure [33] (available at: http://cng.gmu.edu:8080/Lm/). Spines were detected using the Rayburst-based spine analysis routine of NeuronStudio [19, 25, 30, 31]. Classification was based on the absence or presence of a spine neck, on the spine head diameter, and on length. Spines without a neck were classified as "stubby". Spines with necks were classified as "thin" if they had a head diameter of ≤0.6 µm and as "mushroom" if their head diameter was >0.6 µm. Finally, spines >3 µm in length were classified as filopodia.

Light and electron microscopy

Mice used for the light and electron microscopy studies were deeply anesthetized with sodium pentobarbital (I.P.) and then perfused transcardially with a fixative solution of 1% paraformaldehyde and 1.25% glutaraldehyde in 0.1 M cacodylate buffer at pH 7.2–7.4 and 37°C. Brains were removed and 1-mm thick slices were obtained from the dorsal premotor cortex at the anteroposterior level between the anterior commissure and the hippocampus. For each subject, 3–4 blocks of tissue were prepared for light and electron microscopic examination as previously described [11]. One-micron sections were cut with an RMC MT6000-XL ultramicrotome using a glass knife, mounted on glass slides and stained at 60°C for 2 min with 1% toluidine blue. These sections were used for assessment of cortical thickness and relative neuron number in TG versus NT frontal cortex. Using a 40× objective, 270-µm wide columns of neurons with visible nuclei, extending from the pial surface to subcortical white matter in the dorsal premotor (frontal) cortex were counted. Cortical thickness was defined as the distance between the pial surface and the interface between cortex and subcortical white matter. Thin sections for electron microscopy were cut and mounted on copper grids, then stained using uranyl acetate and lead citrate. Thin sections were examined and photographed using a JEOL 100S electron microscope (JEOL USA, Peabody, MA, USA) and photographic negatives were scanned at 800 dpi using an Epson Perfection V700 photo scanner. Estimation of the numerical density of synapses and size of postsynaptic densities was performed using the size frequency method as described previously [20].

Cell inclusion criteria and statistical analyses

For electrophysiological recordings with cell filling, 6–8 frontal cortical slices were prepared from each animal. Electrophysiological data were obtained from 0 to 3 cells per slice and a maximum of 2 cells in any given slice met both electrophysiological and morphological inclusion criteria. A total of 15 TG and 11 NT cells met *both* stringent electrophysiological and morphological inclusion criteria. Of the TG cells, seven contained an NFT and eight did not contain an NFT. Electrophysiological criteria were: (1) a resting membrane potential of ≤−55 mV; (2) stable access resistance; (3) an AP overshoot, and; (4) ability to fire repetitive APs during prolonged depolarizing current

steps. Morphological criteria were: (1) an intact soma; (2) a completely filled dendritic arbor, including spines, and; (3) no cut dendrites in the proximal third of the apical dendritic arbor. For assessment of synaptic physiological properties, cells that met electrophysiological criteria, but were not morphologically studied in detail, were also included in this dataset to improve statistical power. Thus for synaptic physiological studies, a total of 22 TG and 28 NT cells were analyzed. Statistical comparisons of electrophysiological and morphological data from TG versus NT cells were performed in Excel (two-tailed Student's *t*; two-tailed Dunnett's *t*), Prism (Chi-squared tests) and MiniAnalysis (Kolmogorov–Smirnov tests). Results are expressed as mean ± standard error of the mean and significance defined at the $p < 0.05$ level.

Results

Object recognition is impaired in TG mice

Rodents exhibit object recognition memory by exploring novel objects more than they do familiar objects. Furthermore, when a familiar object is placed in a novel location, exploration of the object is greater than if the object remains in the familiar location (indicating object-in-place or "where" memory). To assess object recognition memory of mice in the present study, discrimination ratios (time spent exploring familiar/novel objects or familiar object-familiar location/familiar object-novel location) were calculated using Phase 3 data (Fig. 1).

Figure 1 illustrates the mean discrimination ratios for NT and TG subjects for objects in either their original (O) or a new (N) location and following either a 5- or a 15-min delay interval. If the subjects explored all the objects equally, independent of time or location, their discrimination ratios would fall at chance levels (25%, indicated by the dashed line in Fig. 1). First, to determine the effect of the delay interval on object recognition ("what" aspect of memory), Dunnett two-tailed *t* tests were performed which compared the subject's discrimination ratios at 5- versus 15-min delay intervals for objects that remained in their original location. While delay interval had no significant effect on the percent of time the NT subjects spent exploring the objects, this was not the case for the TG mice. TG mice spent a significantly greater percent of their time investigating the objects following the 15-min delay when compared with the 5-min delay ($p < 0.05$). This finding indicates that with a longer delay, the TG mice were significantly impaired in their ability to remember that they had seen the object before.

A difference between groups was also observed when the location of the object was taken into consideration.

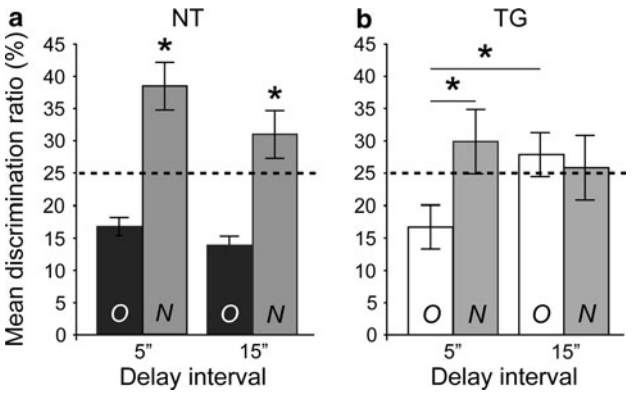

Fig. 1 Object recognition is impaired in TG mice. **a** Mean discrimination ratios for NT mice for objects in the original (O) or novel (N) location following either a 5- or 15-min delay interval. Mean discrimination ratios for objects in the original location were comparable following 5- and 15-min delay intervals. Objects in a novel location were explored significantly more than objects in the original location following both 5- and 15-min delay intervals. **b** TG mice explored objects in the original location for a significantly greater percentage of time after a 15-min compared to a 5-min delay interval, but discrimination ratios for objects in original and novel locations following a 15-min delay did not differ. *Dashed line*: chance level. *$p < 0.05$; two-tailed Dunnett's *t* test; *n*: 5 NT, 6 TG mice

Following a 5-min delay, both the TG and NT mice showed a significant increase in the amount of time they spent exploring an object when it was in a new location ($p < 0.05$), indicating that following a 5-min delay interval, both TG and NT were capable of object-in-place ("where") type recognition. However, following the 15-min delay interval, only the NT mice exhibited this increase ($p < 0.05$), while TG exhibited no significant preference for exploring the object in its new location. Because the prefrontal cortex has been shown to play a critical role in this type of "object-in-place" memory using the object recognition test [1, 6], this lack of "where" type recognition in the TG mice can be interpreted as an indication that the neurodegeneration seen in the frontal cortex of these animals negatively impacts some aspects of their episodic memory function.

Significant tau pathology in the frontal cortex of TG mice

We assessed the degree of tauopathy in the experimental subjects by examining frontal cortical thickness, neuron numbers and presence of neurofibrillary tangles (NFTs), and basic morphological and physiological properties of frontal cortical layer 3 pyramidal cells. Significant cortical shrinkage, neuron loss, and NFTs in the neocortex of 8- to 9-month-old rTg4510 mice have previously been established [32, 36]. In the cohort of TG mice in the

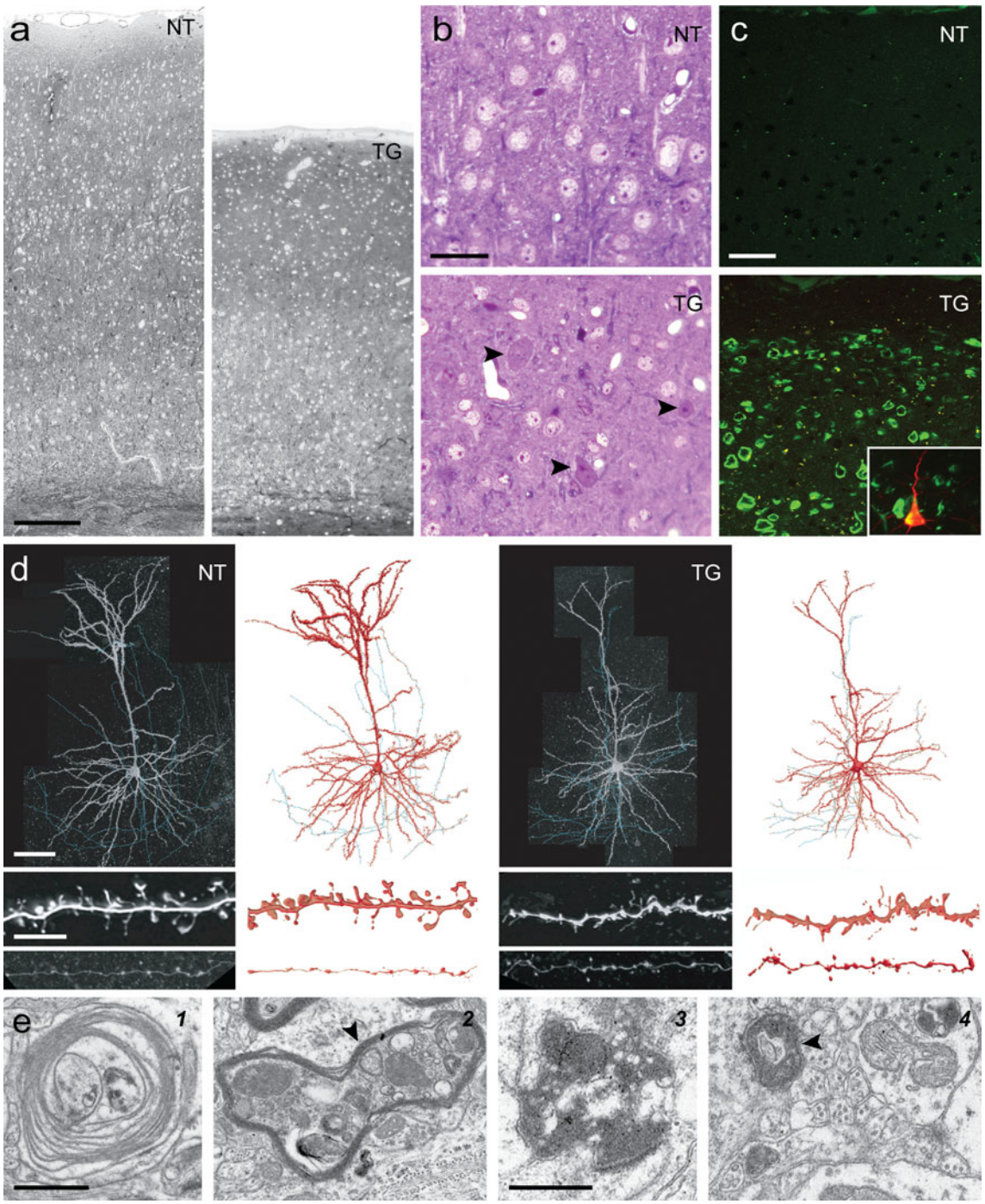

Fig. 2 Advanced tau pathology in TG mice. **a** Low magnification photomicrographs of NT and TG dorsal premotor frontal cortex. Grey matter thickness is notably reduced in TG cortex. **b** Higher magnification photomicrographs of NT and TG cortex. Pyknotic nuclei characteristic of degenerating neurons (*arrowheads*) are common in TG cortex. **c** Thioflavin-S stained cortex showing abundant mature NFTs in TG cortex. *Inset* layer 3 pyramidal cell filled with biocytin during recording and subsequently labeled with streptavidin-Alexa 546 (*red*). The cell contains a Thioflavin-S positive inclusion in the soma (*yellow*). **d** Tiled confocal stacks of NT and TG cells (*top panels*), and representative dendritic (*middle panels*) and axonal segments (*bottom panels*) sampled for dendritic spine and bouton assessment. To the *right* of the confocal images are corresponding NeuronStudio reconstructions of the same cells and axonal and dendritic segments. **e** Electron micrographs demonstrating degenerating profiles in the cortex of a 9-month-old TG mouse, including, (1) a dystrophic axon with split myelin sheath; (2) a dystrophic axon; (3) degenerating axonal boutons, and; (4) a degenerating dendritic spine. *Scale bars* **a** 100 μm; **b**, **c** 20 μm, **d** *top panels*, 40 μm; *middle* and *bottom panels*, 5 μm; **e** *Panels 1* and *2*, 1 μm; *panels 3* and *4*, 0.5 μm

present study, dorsal premotor frontal cortical grey matter thickness was reduced by 33% and the number of neurons was reduced by approximately 30% (Fig. 2a, b), and many thioflavin-S positive NFTs were present (Fig. 2c). As we previously reported [28], dendritic regression occurred in layer 3 pyramidal cells from TG mice (Figs. 2d, 5a). At the ultrastructural level, myelin and axon dystrophy and degenerating axonal boutons and spines were observed (Fig. 2e).

TG cells were more excitable than NT cells, with significantly depolarized resting membrane potentials and increased firing rates in response to depolarizing current steps. Electrophysiological data for the morphologically characterized cells in the present study are presented in Table 1. Because no significant difference in the morphology or physiology of tangle bearing versus non-tangle bearing TG cells was observed [as in Ref. 28] these cells were grouped for statistical analyses.

Table 1 Basic electrophysiological properties

	NT	TG	p[a]
Resting potential (mV)	−77.1 ± 2.0	−67.9 ± 1.7	*0.002*
Membrane time constant (ms)	26.6 ± 3.7	37.6 ± 6.3	0.62
Input resistance (MΩ)	152 ± 29	236 ± 34	0.33
AP firing rate[b] (Hz)	6.7 ± 2.7	13.7 ± 1.3	*0.02*

[a] Student's t test

[b] In response to a 180 pA current step

Significant reduction in dendritic diameter in TG cells

We previously demonstrated that a majority of frontal cortical layer 3 pyramidal cells examined in TG mice exhibit dendritic regression, most prominently in the distal-apical region [28]. Significant dendritic thinning also occurs, and is accompanied by an increased prevalence of dystrophic neurites with varicosities. The presence of the latter, and the fact that dendrites taper markedly in a somatofugal manner, precludes simple assessment of average diameter of dendritic branches. Thus the dendritic diameters for distal-apical, mid-apical and basilar dendritic segments (Fig. 3a, b) were plotted as cumulative distribution histograms (0.05 μm bins; Fig. 3c). No significant difference in the diameter distribution was observed for distal-apical branches in NT versus TG cells. TG cells had a significantly higher proportion of thin (<0.5 μm diameter) mid-apical dendrites compared to NT cells ($p < 0.0001$), and a trend toward a higher proportion of thin (<0.3 μm) basilar dendrites ($p < 0.08$).

Significant reduction in density of dendritic spines in TG cells is due to a specific loss of mushroom spines

Total spine density was decreased by 25% in the apical dendritic arbor of TG cells (0.9 ± 0.1 in TG vs. 1.2 ± 0.1 spines/μm in NT; $p = 0.05$) and a similar reduction (23%) was observed in the basal dendritic arbor (1.1 ± 0.1 spines/μm in TG vs. 1.4 ± 0.1 spines/μm in NT; $p = 0.06$). Spine

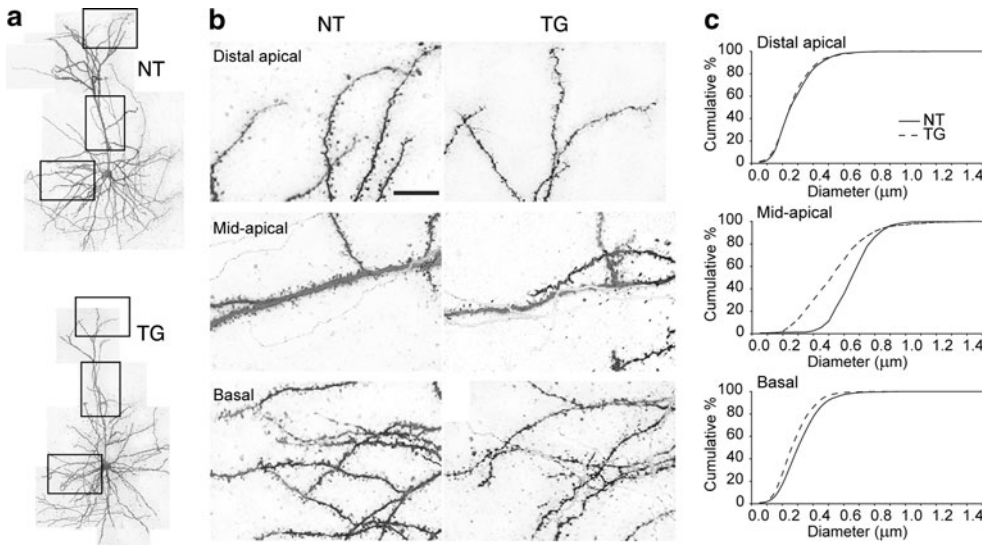

Fig. 3 Reduced dendritic diameter in TG cells. **a** Tiled confocal image stacks of representative NT and TG cells. *Boxed areas* indicate regions from which dendritic segments were sampled for diameter assessment. **b** Confocal images of distal apical, mid-apical, and basal dendrites. **c** Cumulative distribution histograms (0.05 μm bins) of the diameters of distal apical, mid-apical, and basal dendritic segments of NT and TG cells. Diameter distribution of distal apical branches did not differ between NT and TG cells, but TG cells had a significantly higher proportion of thin mid-apical dendrites versus NT cells ($p < 0.0001$; Chi-square test), and there was a trend toward a higher proportion of thin basilar dendrites in the TG versus NT cells ($p < 0.08$; Chi-square test). *Scale bar* **b** 20 μm; n: 15 TG, 11 NT cells

density on the mid-apical dendritic shaft was not different between cells from the two groups (2.0 ± 0.1 spines/μm in TG vs. 2.1 ± 0.3 spines/μm in NT).

To determine whether specific spine subtypes were preferentially vulnerable, we assessed the relative proportion of spine subtypes (percentage of total spines) along dendrites of TG versus NT cells. This analysis revealed a significant reduction in the proportion of mushroom-type spines in the distal-apical ($p < 0.0004$), and basal dendritic arbors ($p < 0.02$), but not the mid-apical branches of TG cells (Fig. 4). Interestingly, there was also an increase in the relative proportion of filopodia-type spines along both distal and mid-apical ($p < 0.01$ and $p = 0.01$, respectively) but not basal dendrites of TG cells (Fig. 4). There was no difference in the proportion of thin or stubby spines along dendrites of TG compared to NT cells, with the exception of a decreased proportion of stubby spines in the mid-apical arbor ($p < 0.05$; Fig. 4).

Increased spontaneous synaptic activity in TG cells

To examine the functional consequences of advanced tauopathy on the network synaptic properties of cortical neurons, we examined spontaneous excitatory and inhibitory synaptic currents (sEPSCs and sIPSCs) with whole-cell voltage-clamp recordings. Electrophysiological traces of sEPSCs and sIPSCs from representative NT and TG cells are shown in Fig. 5a. The kinetics of sEPSCs were not significantly different between NT and TG cells (rise time, NT: 1.23 ± 0.06 ms; TG: 1.22 ± 0.06 ms and decay time, NT: 6.71 ± 0.47 ms; TG: 6.93 ± 0.65 ms; Fig. 5b, top). The kinetics of sIPSCs were also not significantly different between NT and TG cells (rise time, NT: 2.85 ± 0.57 ms; TG: 2.49 ± 0.53 ms and decay time, NT: 14.23 ± 2.85 ms; TG: 14.37 ± 3.06 ms; Fig. 5b, bottom). These findings demonstrate that the kinetics of AMPA-receptor and $GABA_A$-receptor gating are not changed at this advanced stage of tauopathy.

The mean frequency of sEPSCs was significantly increased in TG relative to NT cells (Fig. 5c, left; $p < 0.04$), but there was no difference in the mean frequency of sIPSCs (Fig. 5c, left). The mean amplitude of sEPSCs did not differ in cells from the two groups (Fig. 5c, right), however, the mean amplitude of sIPSCs was significantly higher in TG relative to NT cells (Fig. 5c, right; $p < 0.05$). In order to gain insight into the relative event amplitude distributions of sEPSCs and sIPSCs in TG versus NT cells, cumulative amplitude plots of data from all TG versus all NT cells were generated (Fig. 5d, left and right, respectively). There was a significant increase in the proportion of small amplitude (<20 pA) sEPSCs in TG compared to NT cells ($p < 0.01$). Conversely there was a significant increase in the proportion of large amplitude (>40 pA) sIPSCs in TG cells ($p < 0.0001$). The excitation–inhibition ratio was calculated for the frequency of the synaptic events in the same cells (sEPSC/sIPSC), and was

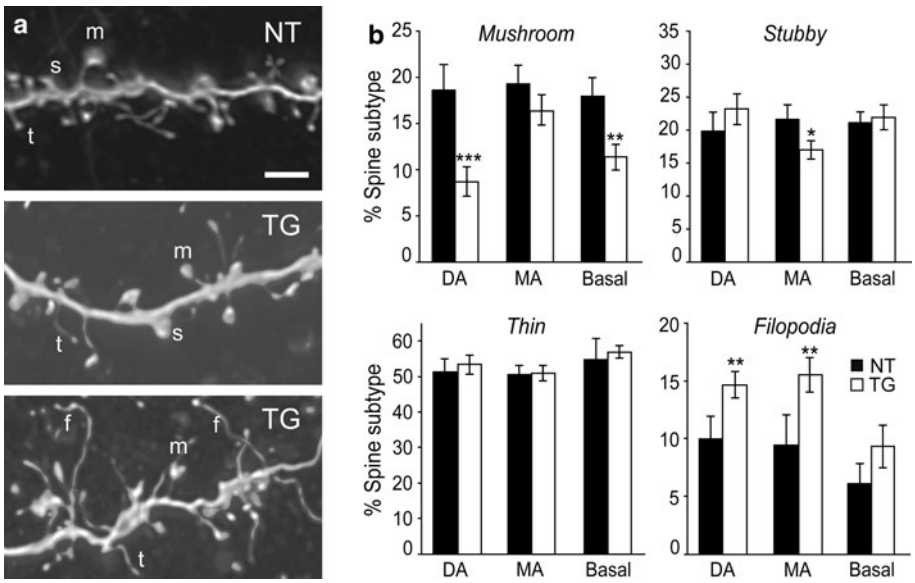

Fig. 4 Decreased mushroom spines and increased filopodia in TG cells. **a** Representative high-resolution ×100 confocal image stacks of dendritic segments used for assessment of spine subtypes. Exemplar spine subtypes are labeled (*m* mushroom, *t* thin, *s* stubby, *f* filopodia). Representative dendritic segments from a NT (*top*) and a TG (*middle*) cell indicate a reduction in total spine density along TG dendrites. Regions of TG dendrites with abundant filopodia were common (*bottom*). **b** *Bar graphs* of mean percent composition of spine subtypes in distal apical (DA), mid-apical (MA), and basal dendrites in NT and TG cells. $*p < 0.05$; $**p < 0.02$; $***p < 0.0004$; two-tailed Student's *t* test; *Scale bar* 2 μm; *n*: 15 TG, 11 NT cells

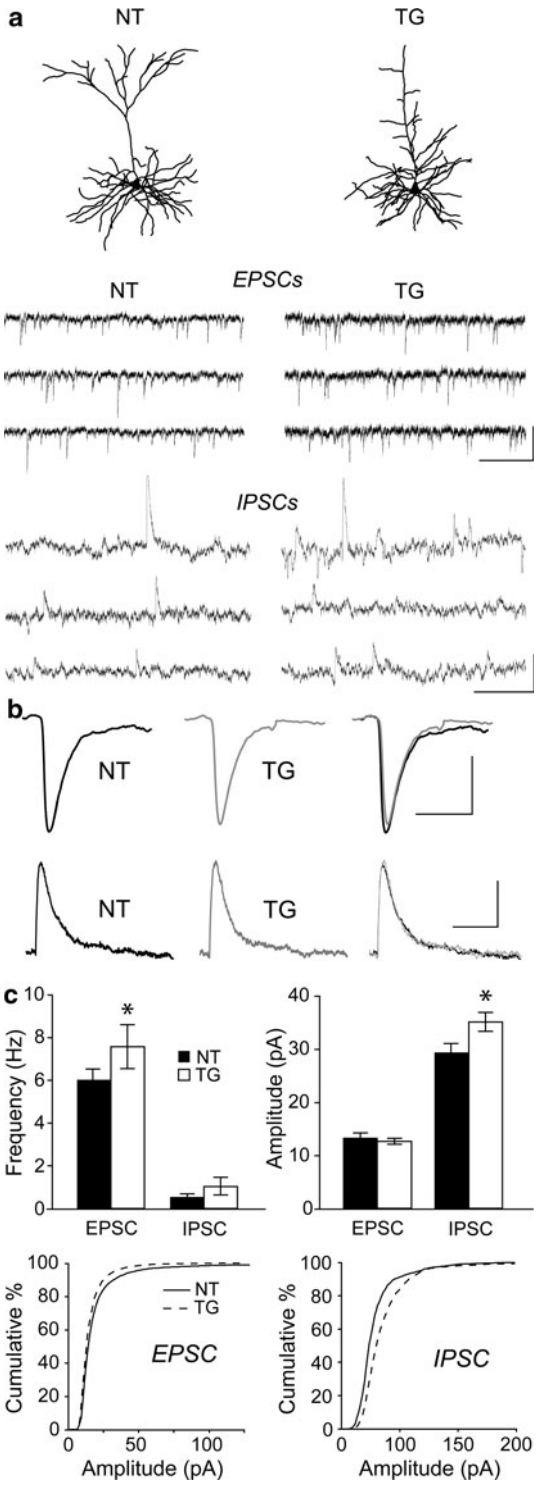

◀ **Fig. 5** Increased frequency of sEPSCs and no change in frequency of sIPSCs in TG cells. **a** Reconstructions of representative cells from which whole-cell voltage-clamp recordings of spontaneous postsynaptic currents were obtained. Representative spontaneous excitatory postsynaptic currents (sEPSCs) and spontaneous inhibitory postsynaptic currents (sIPSCs). **b** Averaged traces of excitatory and inhibitory synaptic currents from cells shown in **a**. Superimposed averaged traces (*right*) indicate no significant difference in the kinetics of either sEPSCs or sIPSCs between NT and TG cells. **c** *Bar graphs* of mean frequency and amplitude of sEPSCs and sIPSCs in NT and TG cells. **d** Cumulative distribution histograms (1 pA bins) of sEPSC and sIPSC amplitudes from NT versus TG cells. The Kolmogorov–Smirnov test revealed a significant increase in the proportion of small amplitude sEPSCs ($p < 0.01$) and large amplitude sIPSC ($p < 0.0001$) in TG cells compared to NT cells. *$p < 0.05$ two-tailed Student's t test. *Scale bars* **a** top 10 pA and 200 ms, **a** bottom 40 pA and 200 ms; **b** top 2 pA and 10 ms, **b** bottom 15 pA and 10 ms; n: 22 TG, 28 NT cells

not significantly different in NT versus TG cells (not shown).

Increased density of axonal boutons in TG cells

To assess possible anatomical mechanisms of maintained or increased synaptic responses in surviving neurons in the frontal cortex of mice in which a large number of neurons had died and stable spines lost, we sought to determine whether presynaptic (boutons) as well as postsynaptic (spines) entities were altered. The axonal plexuses of neurons from which recordings were obtained were very well filled (on average more than 5,000 μm of axon per cell could be reconstructed) which allowed assessment of density of axonal boutons (Fig. 6a). Axons of TG cells showed a significant increase in mean density of axonal boutons compared to NT cells ($p < 0.02$) with increases in both terminaux ($p < 0.04$) and en passant bouton types ($p = 0.06$).

Increased density of asymmetric synapses and reduced size of post-synaptic densities in the neuropil of TG mice

To gain further understanding of mechanisms of maintained synaptic function during advanced-stage tauopathy, we examined individual excitatory (asymmetric) and inhibitory (symmetric) synapses in layer 3 frontal cortical neuropil from TG and NT mice (Fig. 7a). The majority of the synapses were asymmetric, and characterized by a postsynaptic density (PSD) in both TG and NT mice (Fig. 7b1). The numerical density of asymmetric synapses (number per unit volume) was increased in TG neuropil ($p = 0.06$) while the numerical density of symmetric synapses was unchanged (Fig. 7b1). We next assessed the relative proportion of axospinous and axodendritic asymmetric synapses, and found no difference between TG and NT mice (Fig. 7b2). There was no difference in the relative proportion of asymmetric synapses with simple or perforated PSDs between the two groups (Fig. 7b3). The mean PSD length was significantly shorter in TG neuropil (0.28 ± 0.01 μm) compared to NT (0.33 ± 0.01 μm; $p < 0.01$). PSD length was plotted as a cumulative distribution histogram, which revealed a significantly higher

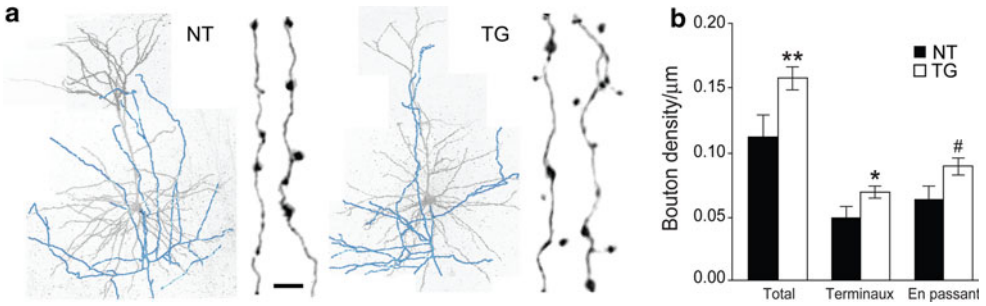

Fig. 6 Increased density of axonal boutons in TG cells. **a** Tiled confocal image stacks (*inverted*) of representative NT and TG cells with reconstructions of axonal arbors indicated in *blue*. High magnification images of representative axonal segments are shown to the *right*. **b** *Plots* of mean density of total, 'terminaux' and 'en passant' boutons in TG versus NT cells. $^{\#}p = 0.06$; $^{*}p < 0.04$; $^{**}p < 0.02$; two-tailed Student's *t* test; *Scale bar* **a** 2 µm; *n*: 8 TG, 4 NT axons

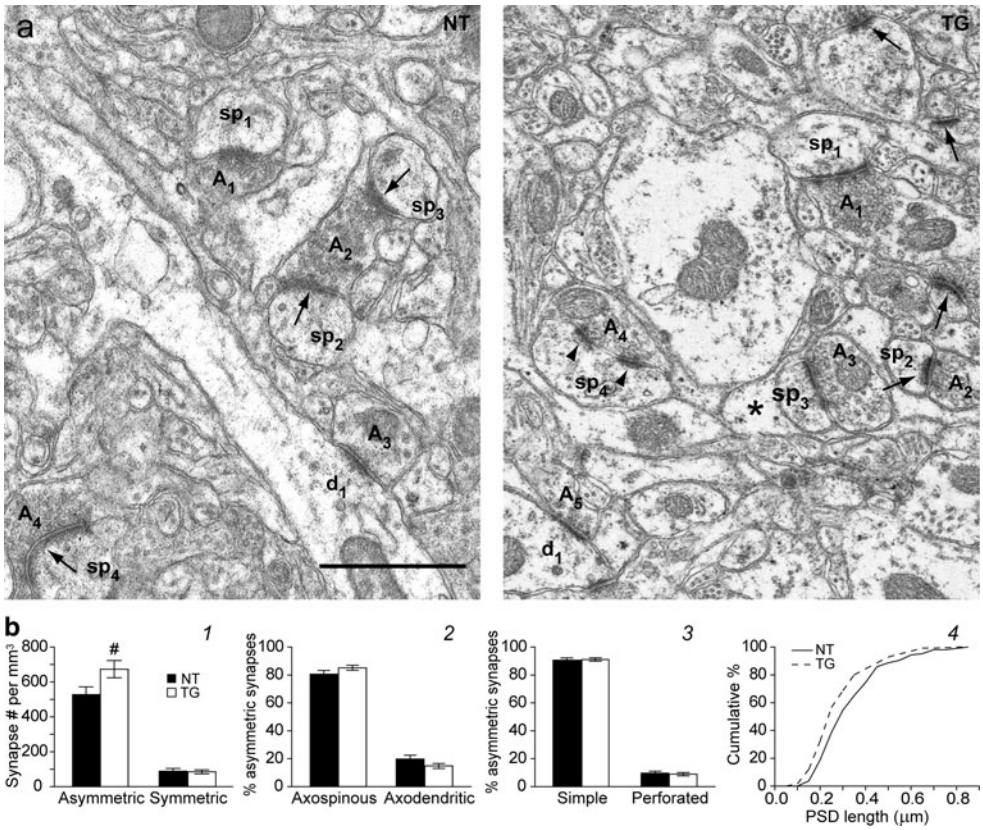

Fig. 7 Increased density but reduced size of asymmetric synapses in TG neuropil. **a** Representative electron micrographs from NT and TG layer 2/3 frontal cortical neuropil. Asymmetric synapses with prominent post-synaptic densities (PSDs) and wide clefts between pre and postsynaptic membranes are readily apparent. In the field of view on the *left* (NT plate), one spine (sp_1) is forming an asymmetric synapse with an axon terminal (A_1). Two additional spines (sp_2 and sp_3) both form asymmetric synapses with the same axon terminal (A_2). These synapses, in addition to that formed between a fourth spine (sp_4) and another axon terminal (A_4), have PSDs that are characteristic in length of those found at NT synapses (*arrows*). A dendrite (d_1) also forms an asymmetric synapse with an axon terminal (A_3). In the field of view on the *right* (TG plate) a spine (sp_1) forms an asymmetric synapse with an axon (A_1). While this spine contains a PSD that is comparable in length to many of those found at NT synapses (*left panel*, *arrows*), the PSD at another spine (sp_2) forming an asymmetric synapse with an additional axon terminal (A_2) is shorter in length. There are a higher proportion of shorter PSDs in TG neuropil (*arrows*) compared to NT neuropil. An astrocytic end-foot (*asterisk*) can be seen encircling a synapse between a third spine (sp_3) and axon terminal (A_3) pair. A perforated PSD (*arrowheads*) is located at another spine (sp_4) that forms an asymmetric synapse with another axon terminal (A_4). A dendrite (d_1) can also be seen in this field of view forming an asymmetric synapse with an axon terminal (A_5). **b** *1* Mean synapse number per mm^3 (± SEM) for asymmetric and symmetric synapses in TG compared to NT neuropil. *2* Relative proportion of axospinous and axodendritic asymmetric synapses in NT compared to TG neuropil. *3* Relative proportion of simple and perforated asymmetric synapses. *4* Cumulative distribution histograms (0.05 µm bins) of PSD length at TG and NT asymmetric synapses. There was a significantly higher proportion of shorter PSDs in TG versus NT neuropil ($p < 0.01$; Chi-square test). *Scale bar* **a** 1 µm; $^{\#}p = 0.06$; two-tailed Student's *t* test

proportion of shorter PSDs in TG neuropil compared to NT neuropil (0.1 μm bins; $p < 0.01$; Fig. 7b4).

Discussion

The strong association of synapse loss with cognitive impairment in Alzheimer's disease [38] and evidence for early and progressive synaptic alterations in mouse models of AD and other tauopathies has led to the widely held view of these neurodegenerative diseases as synaptopathies [45]. However, given the relatively slow time course of neurodegenerative tauopathies, synaptic degradation and dysfunction are not likely to follow a simple downward linear path during disease progression. Rather, it is likely that surviving neuronal networks compensate for neuron and synapse loss through homeostatic mechanisms that maintain relatively normal network activity for a period of time [35]. We took advantage of the rTg4510 mouse model of progressive tauopathy to examine synaptic function at an advanced stage of pathology, when extensive neuron loss leads to significant disruption of cortical networks. It has been established that by 9 months in these mice, the cortex has thinned, up to 50% of neurons have been lost, and NFTs are abundant [36]—all changes that were present in our experimental subjects. These global changes alone predict significant perturbations in cortical network function. However, we also observed, here and previously [28], significant structural changes to surviving neurons that would lead to even more severe network dysfunction. These changes include dendritic regression and thinning, loss of mushroom spines, and degeneration of spines and boutons. On the other hand, an increase in filopodia and an increase in density of presynaptic boutons and asymmetric synapses were also observed. At a behavioral level, TG mice were capable of low (5-min delay)—but not high (15-min delay)—demand recognition memory tasks, indicating that frontal cortical networks are impaired but at least partially functional in advanced-stage TG mice.

Synaptic function is not reduced in advanced-stage tauopathy, despite significant degradation of presynaptic and postsynaptic elements

Degenerative and regressive changes at the advanced stage of tauopathy studied here predict that synaptic transmission should be reduced in surviving neurons. For example, since most inputs to layer 3 pyramidal cells arise from local cortical circuits (review [15, 18]) it is difficult to imagine a scenario in which the loss of up to 50% of cortical neurons would not result in significant deafferentation of surviving neurons. Significant deafferentation, in the absence of compensatory response, should lead to reduction in postsynaptic response frequency and amplitude. Further, passive cable theory [26] predicts that the reduced dendritic diameter in TG neurites would result in a reduced length constant due to increased axial resistance. An increase in proportion of thin dendrites across a neuronal arbor would be expected, all other things being equal, to result in a reduced frequency and amplitude of synaptic currents due to increased attenuation of signals traversing the dendritic arbor. Further, a decreased total spine density would be expected to result in decreased synaptic currents measured at the soma.

Despite the many reasons to expect a reduction in synaptic responses in surviving neurons in TG mice, we found that, to the contrary, glutamatergic sEPSCs were increased in frequency and unchanged in amplitude, while sIPSCs were unchanged in frequency and increased in amplitude. Importantly, while the mean amplitude of sEPSCs did not differ in TG cells, there was a significantly higher proportion of small amplitude events. Moreover, the ratio of sEPSC to sIPSC frequency in surviving TG cells was indistinguishable from NT cells, indicating intact excitation/inhibition balance. Thus, it is likely that at an advanced stage of tauopathy surviving networks of pyramidal cells compensate for an initial loss of inputs by increasing synaptic signaling to maintain network stability.

Evidence for homeostatic mechanisms in advanced-stage tauopathy

How is it possible that excitatory synaptic transmission is increased despite substantial structural alterations that predict depressed synaptic responses in TG cells? We propose that as tauopathy progresses in the cortex, surviving neuronal networks respond to deafferentation with homeostatic responses that enable surviving neurons and networks to maintain stable function despite significant perturbations in afferent synaptic inputs and structural changes (Fig. 8). Evidence for homeostatic plasticity has been provided by studies showing that neurons in culture respond to activity blockade (functional deafferentation) by increasing the numbers of postsynaptic AMPA receptors without altering presynaptic glutamate release [10, 17, 42]. Other studies have demonstrated compensatory changes in presynaptic mechanisms (with or without postsynaptic changes) that maintain stable network activity in the face of reduced activity [2, 16, 39, 40].

Data presented here are consistent with the idea that synaptic network homeostasis, which promotes an increase in synaptic signaling in a highly disrupted network, is accomplished at this advanced stage of tauopathy through multiple mechanisms. These include increased excitability of surviving neurons, sprouting of new axonal boutons and filopodia and formation of new synapses.

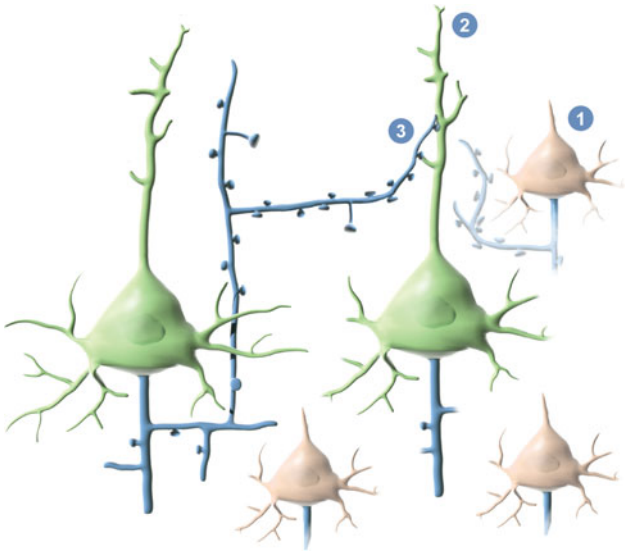

Fig. 8 Proposed model of homeostatic plasticity in cortical pyramidal cells in tauopathy. As tauopathy progresses in the cortex, neurons die (*1*) by an as yet unknown mechanism, leading to deafferentation of surviving neurons. Surviving neurons respond to deafferentation by dendrite and spine regression (*2*, "loss of function") and also with sprouting of new axonal boutons and filopodia and formation of new synapses (*3*, "gain of function"). These homeostatic responses, together with increased excitability, enable surviving neurons and networks to maintain stable function despite significant perturbations in afferent synaptic inputs and structural changes

Increased excitability of surviving neurons results in increased neurotransmitter release

We previously demonstrated that the increased excitability of TG neurons at ~9 months of age is due to a substantially depolarized resting membrane potential in these neurons, which are thus closer to the threshold for action potential generation [28]. Why TG neurons are more depolarized is unclear, although it is plausible that the presence of depolarizing currents such as the H current in the soma at higher densities than normal (unpublished observation) due to impaired trafficking of HCN channels could contribute. Regardless of mechanism, the increase in excitability of surviving neurons likely results in an increase in action potential-dependent release of neurotransmitter from presynaptic terminals [2].

Sprouting of new axonal boutons and filopodia by surviving neurons

Axon sprouting and dystrophy occurs in neurodegenerative diseases, including Alzheimer's disease, and it also occurs in response to experimentally induced lesions in the CNS (review [3]). The present study shows sprouting of axonal boutons and an increase in the density of synapses in the neuropil of TG mice. These changes, along with the increased excitability of the surviving neurons, likely lead to increased frequency of sEPSCs in TG cells. Where might these newly generated synapses occur? In surviving TG cells there is some contraction of dendrites and a decrease in the density of spines, especially mushroom spines, along the remaining dendrites. However, there is a significant increase in filopodia, which do not normally exist in abundance in adult cells and are thus likely generated in response to deafferentation of the parent dendrite. The asymmetric synapses formed by filopodia have short PSD profiles and these probably account for the increased density of synapses in the neuropil of the TG mice, especially since filopodia often form multiple synapses [7, 21, 23]. It is possible that filopodial synapses are formed by new axonal boutons generated by surviving pyramidal neurons. Further, while the mean sEPSC amplitude was not significantly different between TG versus NT cells, cumulative amplitude distributions revealed a significant increase in the proportion of small amplitude events in TG cells. Since the amplitude of a given synaptic event is proportional to the size of a given synapse, this finding is also consistent with the higher proportion of short PSDs in the neuropil of TG mice.

Other mechanisms

Other homeostatic compensatory mechanisms exist in functionally deafferented systems (review [44]), which may also play a role in maintaining function at advanced stages of tauopathy. These include insertion of new AMPAR or other ion channels on remaining spines and dendrites. It is also possible that changes in the synthesis and release of signaling molecules known to play an important role in synaptic scaling, such as BDNF and TNF-α, are altered during tauopathy [35]. Future studies will examine these possibilities. Another possible mechanism is an increase in the proportion of axo-dendritic versus axo-spinous synapses; however, this would be expected to lead to larger, not smaller amplitude events measured at the soma [34]. Further, no differences in the proportion of axo-spinous and axo-dendritic synapses were seen in TG neuropil. Other, as yet unidentified mechanisms may also play a role in maintenance of synaptic function in the TG mice.

Conclusions

In summary, we have demonstrated that synaptic responses in TG cortical pyramidal cells are not reduced at an advanced stage of tauopathy when network degeneration is pronounced, and presented evidence for several plausible homeostatic mechanisms by which synaptic excitation

could be maintained. It is likely that neurons maintain near normal function until pathology reaches a stage that overwhelms compensatory mechanisms, or until compensatory mechanisms themselves become pathological [35].

Acknowledgments We thank Joseph Amatrudo for assistance with data acquisition. Supported by: NIH/NIA R01 AG025062 (J. Luebke); NIH/NINDS R01 NS046355 and Alzheimer's Association IIRG-06-27277 (J. Lewis).

Conflict of interest J. Lewis and Mayo Clinic hold the patent associated with the rTg4510 mice, have a financial interest associated with the rTg4510 mice and have received annual royalties from the licensing of the first technology of greater than the federal threshold for significant financial interest.

References

1. Barker GR, Bird F, Alexander V, Warburton EC (2007) Recognition memory for objects, place, and temporal order: a disconnection analysis of the role of the medial prefrontal cortex and perirhinal cortex. J Neurosci 27(11):2948–2957
2. Burrone J, O'Byrne M, Murthy VN (2002) Multiple forms of synaptic plasticity triggered by selective suppression of activity in individual neurons. Nature 420:414–418
3. Deller T, Haas CA, Freiman TM, Phinney A, Jucker M, Frotscher M (2006) Lesion-induced axonal sprouting in the central nervous system. Adv Exp Med Biol 557:101–121
4. Dere E, Kart-Teke E, Huston JP, De Souza Silva MA (2006) The case for episodic memory in animals. Neurosci Biobehav Rev 30(8):1206–1224
5. DeVito LM, Eichenbaum H (2009) Distinct contributions of the hippocampus and medial prefrontal cortex to the "what-where-when" components of episodic-like memory in mice. Behav Brain Res 215(2):318–325
6. Ennaceur A, Delacour J (1988) A new one-trial test for neurobiological studies of memory in rats. 1: Behavioral data. Behavioral Brain Research 31(1):47–59
7. Fiala JC, Feinberg M, Popov V, Harris KM (1998) Synaptogenesis via dendritic filopodia in developing hippocampal area CA1. J Neurosci 18(21):8900–8911
8. Gendron TF, Petrucelli L (2009) The role of tau in neurodegeneration. Mol Neurodegener 4:13
9. Hoover BR, Reed MN, Su J, Penrod RD, Kotilinek LA, Grant MK, Pitstick R, Carlson GA, Lanier LM, Yuan LL, Ashe KH, Liao D (2010) Tau mislocalization to dendritic spines mediates synaptic dysfunction independently of neurodegeneration. Neuron 68(6):1067–1081
10. Lissin DV, Gomperts SN, Carroll RC, Christine CW, Kalman D, Kitamura M, Hardy S, Nicoll RA, Malenka RC, von Zastrow M (1998) Activity differentially regulates the surface expression of synaptic AMPA and NMDA glutamate receptors. Proc Natl Acad Sci USA 95:7097–7102
11. Ludvigson AE, Luebke JI, Lewis J, Peters A (2011) Structural abnormalities in the cortex of the rTg4510 mouse model of tauopathy: a light and electron microscopy study. Brain Struct Funct 216(1):31–42
12. Luebke JI, Chang YM, Moore TL, Rosene DL (2004) Normal aging results in decreased synaptic excitation and increased synaptic inhibition of layer 2/3 pyramidal cells in the monkey prefrontal cortex. Neuroscience 125(1):277–288
13. Luebke JI, Rosene DL (2003) Aging alters dendritic morphology, input resistance, and inhibitory signaling in dentate granule cells of the rhesus monkey. J Comp Neurol 460(4):573–584
14. McKinney RA (2010) Excitatory amino acid involvement in dendritic spine formation, maintenance and remodelling. J Physiol 588(Pt 1):107–116
15. Morrison JH, Hof PR (2002) Selective vulnerability of corticocortical and hippocampal circuits in aging and Alzheimer's disease. Prog Brain Res 136:467–486
16. Murthy VN, Schikorski T, Stevens CF, Zhu Y (2001) Inactivity produces increases in neurotransmitter release and synapse size. Neuron 32:673–682
17. O'Brien RJ, Kamboj S, Ehlers MD, Rosen KR, Fischbach GD, Huganir RL (1998) Activity-dependent modulation of synaptic AMPA receptor accumulation. Neuron 21:1067–1078
18. Peters A (2002) Examining neocortical circuits: some background and facts. J Neurocytol 31:183–193
19. Peters A, Kaiserman-Abramof IR (1970) The small pyramidal neuron of the rat cerebral cortex. The perikaryon, dendrites and spines. Am J Anat 127(4):321–355
20. Peters A, Sethares C, Luebke JI (2008) Synapses are lost during aging in the primate prefrontal cortex. Neuroscience 152(4):970–981
21. Petrak LJ, Harris KM, Kirov SA (2005) Synaptogenesis on mature hippocampal dendrites occurs via filopodia and immature spines during blocked synaptic transmission. J Comp Neurol 484(2):183–190
22. Polydoro M, Acker CM, Duff K, Castillo PE, Davies P (2009) Age-dependent impairment of cognitive and synaptic function in the htau mouse model of tau pathology. J Neurosci 29(34):10741–10749
23. Popov V, Stewart M (2009) Complexity of contacts between synaptic boutons and dendritic spines in adult rat hippocampus: three-dimensional reconstructions from serial ultrathin sections in vivo. Synapse 63(5):369–377
24. Pritchard SM, Dolan PJ, Vitkus A, Johnson GV (2011) The toxicity of tau in Alzheimer disease: turnover, targets and potential therapeutics. J Cell Mol Med (Epub ahead of print)
25. Radley JJ, Rocher AB, Rodriguez A, Ehlenberger DB, Dammann M, McEwen BS, Morrison JH, Wearne SL, Hof PR (2008) Repeated stress alters dendritic spine morphology in the rat medial prefrontal cortex. J Comp Neurol 507:1141–1150
26. Rall W (1969) Time constants and electrotonic length of membrane cylinders and neurons. Biophys J 9(12):1483–1508
27. Ramsden M, Kotilinek L, Forster C, Paulson J, McGowan E, SantaCruz K, Guimaraes A, Yue M, Lewis J, Carlson G, Hutton M, Ashe KH (2005) Age-dependent neurofibrillary tangle formation, neuron loss, and memory impairment in a mouse model of human tauopathy (P301L). J Neurosci 25(46):10637–10647
28. Rocher AB, Crimins JL, Amatrudo JM, Kinson MS, Todd-Brown MA, Lewis J, Luebke JI (2010) Structural and functional changes in tau mutant mice neurons are not linked to the presence of NFTs. Exp Neurol 223(2):385–393
29. Rocher AB, Kinson MS, Luebke JI (2009) Significant structural but not physiological changes in cortical neurons of 12-month-old Tg2576 mice. Neurobiol Dis 32(2):309–318
30. Rodriguez A, Ehlenberger D, Kelliher K, Einstein M, Henderson SC, Morrison JH, Hof PR, Wearne SL (2003) Automated reconstruction of three-dimensional neuronal morphology from laser scanning microscopy images. Methods 30:94–105
31. Rodriguez A, Ehlenberger DB, Hof PR, Wearne SL (2006) Rayburst sampling, an algorithm for automated three-dimensional shape analysis from laser scanning microscopy images. Nat Protoc 1:2152–2161
32. Santacruz K, Lewis J, Spires T, Paulson J, Kotilinek L, Ingelsson M, Guimaraes A, DeTure M, Ramsden M, McGowan E, Forster

C, Yue M, Orne J, Janus C, Mariash A, Kuskowski M, Hyman B, Hutton M, Ashe KH (2005) Tau suppression in a neurodegenerative mouse model improves memory function. Science 309:476–481
33. Scorcioni R, Polavaram S, Ascoli GA (2008) L-Measure: a web-accessible tool for the analysis, comparison and search of digital reconstructions of neuronal morphologies. Nat Protoc 3(5):866–876
34. Segal M (2010) Dendritic spines, synaptic plasticity and neuronal survival: activity shapes dendritic spines to enhance neuronal viability. Eur J Neurosci 31:2178–2184
35. Small DH (2008) Network dysfunction in Alzheimer's disease: does synaptic scaling drive disease progression? Trends Mol Med 14(3):103–108
36. Spires TL, Orne JD, SantaCruz K, Pitstick R, Carlson GA, Ashe KH, Hyman BT (2006) Region-specific dissociation of neuronal loss and neurofibrillary pathology in a mouse model of tauopathy. Am J Pathol 168(5):1598–1607
37. Sydow A, Van der Jeugd A, Zheng F, Ahmed T, Balschun D, Petrova O, Drexler D, Zhou L, Rune G, Mandelkow E, D'Hooge R, Alzheimer C, Mandelkow EM (2011) Tau-induced defects in synaptic plasticity, learning, and memory are reversible in transgenic mice after switching off the toxic Tau mutant. J Neurosci 31(7):2511–2525
38. Terry RD, Masliah E, Salmon DP, Butters N, DeTeresa R, Hill R, Hansen LA, Katzman R (1991) Physical basis of cognitive alterations in Alzheimer's disease: synapse loss is the major correlate of cognitive impairment. Ann Neurol 30(4):572–580
39. Thiagarajan TC, Lindskog M, Tsien RW (2005) Adaptation to synaptic inactivity in hippocampal neurons. Neuron 47:725–737
40. Thiagarajan TC, Piedras-Renteria ES, Tsien RW (2002) alpha- and beta-CaMKII. Inverse regulation by neuronal activity and opposing effects on synaptic strength. Neuron 36:1103–1114
41. Thies E, Mandelkow EM (2007) Missorting of tau in neurons causes degeneration of synapses that can be rescued by the kinase MARK2/Par-1. J Neurosci 27(11):2896–2907
42. Turrigiano GG, Leslie KR, Desai NS, Rutherford LC, Nelson SB (1998) Activity-dependent scaling of quantal amplitude in neocortical neurons. Nature 391:892–896
43. Turrigiano GG, Nelson SB (2004) Homeostatic plasticity in the developing nervous system. Nat Rev Neurosci 5:97–107
44. Turrigiano GG (2008) The self-tuning neuron: synaptic scaling of excitatory synapses. Cell 135:422–435
45. Wishart TM, Parson SH, Gillingwater TH (2006) Synaptic vulnerability in neurodegenerative disease. J Neuropathol Exp Neurol 65(8):733–739
46. Yoshiyama Y, Higuchi M, Zhang B, Huang SM, Iwata N, Saido TC, Maeda J, Suhara T, Trojanowski JQ, Lee VM (2007) Synapse loss and microglial activation precede tangles in a P301S tauopathy mouse model. Neuron 53(3):337–351